RF-SABRE: a Way to Continuous Spin Hyperpolarization at High Magnetic Fields

ARTICLE *in* THE JOURNAL OF PHYSICAL CHEMISTRY B · MAY 2015

Impact Factor: 3.3 · DOI: 10.1021/acs.jpcb.5b03032 · Source: PubMed

RF-SABRE: a Way to Continuous Spin Hyperpolarization at High Magnetic Fields

Andrey N. Pravdivtsev,[1,2] *Alexandra V. Yurkovskaya,*[1,2] *Hans-Martin Vieth,*[3] *Konstantin L. Ivanov*[1,2]

[1] International Tomography Center, Siberian Branch of the Russian Academy of Science, Institutskaya 3a, Novosibirsk, 630090, Russia

[2] Novosibirsk State University, Pirogova 2, Novosibirsk, 630090, Russia

[3] Institut für Experimentalphysik, Freie Universität of Berlin, Arnimallee 14, Berlin, 14195, Germany

KEYWORDS. Spin hyperpolarization, SABRE method, polarization transfer, NMR enhancement

ABSTRACT

A new technique is developed that allows one to carry out the Signal Amplification By Reversible Exchange (SABRE) experiments at high magnetic field. SABRE is a hyperpolarization method, which utilizes transfer of spin order from para-hydrogen to the spins

of a substrate in transient iridium complexes. Previously, it has been thought that such a transfer of a spin order is only efficient at low magnetic fields, notably, at Level Anti-Crossing (LAC) regions. Here it is demonstrated that LAC conditions can also be fulfilled at high fields under the action of an RF-field. The high-field RF-SABRE experiment can be implemented using commercially available Nuclear Magnetic Resonance (NMR) and Magnetic Resonance Imaging (MRI) machines and does not require technically demanding field-cycling. The achievable NMR enhancements are around 100 for several substrates as compared to their NMR signals at thermal equilibrium conditions at 4.7 Tesla. The frequency dependence of RF-SABRE is comprised of well pronounced peaks and dips, whose position and amplitude are conditioned solely by the magnetic resonance parameters such as chemical shifts and scalar coupling of the spin system involved in the polarization transfer and by the amplitude of the RF-field. Thus, the proposed method can serve as a new sensitive tool for probing transient complexes. Simulations of the dependence of magnetization transfer (i.e., NMR signal amplifications) on the frequency and amplitude of the RF-field are in good agreement with the developed theoretical approach. Furthermore, the method enables continuous re-hyperpolarization of the SABRE substrate over a long period of time giving a straightforward way to repetitive NMR experiments.

I. Introduction

Signal Amplification By Reversible Exchange (SABRE) is relatively new and rapidly developing hyperpolarization method[1-14]. In a SABRE experiment a substrate molecule is spin-polarized in a transient complex with parahydrogen, *p*-H_2, which is the H_2 molecule in its singlet spin state, due to a process of spin order transfer, see Scheme 1. The SABRE technique belongs to the family of hyperpolarization methods aimed at increasing the low inherent sensitivity of Nuclear Magnetic Resonance (NMR). In general, NMR techniques, despite their versatility and usefulness, suffer from notoriously low sensitivity, which curbs the range of potential applications. The sensitivity issue is coming from low polarization of nuclear spins at thermal equilibrium, which is usually of the order of 10^{-4}; thus, an efficient method to tackle this problem is using hyper-polarized nuclear spins, i.e., spins shifted far off thermal equilibrium. SABRE is a hyperpolarization technique, which enables strong spin polarization of various molecules and NMR signal enhancements up to several thousands. A further advantage of the SABRE method, recently demonstrated by Hövener et al.[15-16] is that this technique allows continuous re-hyperpolarization of the target substrate molecule: after the strong non-thermal spin order is destroyed by an NMR measurement, under constant supply of *p*-H_2 it is quickly restored within a few seconds. Moreover, successive measurements do not exhibit any significant loss of signal over a few hundreds of acquisitions. This property makes feasible measurements with signal accumulation; this is in contrast with the standard Para-Hydrogen Induced Polarization (PHIP) experiment[17], in which the substrate is chemically modified and cannot be re-polarized.

It has been shown[7-11] that the polarization transfer process among spins, which is in the heart of the SABRE method, is efficient at low fields where the nuclear spins are coupled strongly, meaning that the difference in their Zeeman interactions with the field is smaller than the

coupling strength. Specifically, it is established[7-11] that the SABRE method works efficiently (i.e., produced enhancements from a few 100 up to several 1000 as compared with thermal polarization at a high field of 1-10 Tesla) only at low magnetic fields, specifically [5, 11], only within the regions of nuclear spin energy Level Anti-Crossings (LACs) of the SABRE complex. Typically, such LACs occur at low magnetic fields, below 20 mT[8-9, 18]; in contrast, spontaneous high-field SABRE[19] is based on polarization transfer by cross-relaxation, which is by far less efficient. Since in modern NMR signal detection is usually done at high magnetic field where spectral resolution is the best, the standard SABRE experiment requires field-cycling between a low polarization field and the high detection field. During the field-cycling stage, depending on the lifetime of hyperpolarization, there is an inevitable loss of polarization; furthermore, doing experiments with field-cycling is technically demanding and requires using additional devices for switching the external magnetic field. However, in recent works it has been demonstrated that one can use RF-fields to fulfill LAC conditions at a high magnetic field of an NMR spectrometer or Magnetic Resonance Imaging (MRI) scanner[20-21]. Moreover, in a very recent work[4] we have shown that such high-field LACs enable SABRE experiments at high magnetic fields. This version of the SABRE technique, RF-SABRE, enables fast transfer of spin order (typically, within 1 second) and provides significant NMR signal enhancements. The high-field SABRE technique is based on using an RF-field with carefully set amplitude and frequency: this enables modeling the low-field conditions at high magnetic fields. Thus, RF-SABRE[4] gives a way to circumvent problems originating from the need of doing field-cycling by performing SABRE experiments directly at the high magnetic field of an NMR spectrometer. After this first showcasing example, we are going to describe here the method in more detail and demonstrate that it works efficiently for a wide range of SABRE substrates.

In the article, we (i) explain in detail the physical principles behind RF-SABRE, (ii) present experimental results for high-field SABRE under LAC conditions for four different substrates and two Iridium-based SABRE complexes and (iii) demonstrate that RF-SABRE also allows one to generate hyperpolarization in a continuous way with high efficiency. Advantages and potential applications of the method, which is an important step in developing high-field SABRE, are also discussed, as well as factors limiting the presently achieved NMR signal enhancement.

II. Methods

A. Sample preparation

As SABRE substrates we used pyridine (Py), 4,4′-bipyridine, 2,2′-bipyrazine and 3-methyl-1H-pyrazole; see the structures of the substrates in Chart 1. We used two types of SABRE pre-catalyst: IrIMesCODCl (IMes=1,3-bis(2,4,6-trimethylphenyl) imidazole-2-ylidene, COD=cyclooctadiene)[9] and Crabtree's catalyst, $IrP(C_6H_{11})_3PyCOD]PF_6$[22]. In experiments with Py two different samples were used. Sample 1 contained 70 mM of Py and 4 mM IrIMes methanol-d_4 (MeOD). Sample 2 contained 70 mM of Py and 4 mM of Crabtree's catalyst in MeOD. In experiments with the other substrates we always used the IrIMesCODCl pre-catalyst and prepared the following samples: 20 mM of 4,4′-bipyridine and 4 mM of IrIMesCODCl in MeOD; 6 mM of 2,2′-bipyrazine and 4 mM of IrIMesCODCl in a mixture of 80% MeOD and 20% DMSO; 60 mM of 3-methyl-1H-pyrazole and 4 mM of IrIMesCODCl in MeOD. Crabtree's catalyst was purchased from ABCR GmbH; IrIMesCODCl was synthesized using a procedure described before[23]; methanol-d_4 was purchased from Deutero GmbH; all other compounds were purchased from Sigma Aldrich. Samples were prepared without additional purification. Parahydrogen was enriched using a Bruker parahydrogen generator yielding a content of 92 % *p*-H_2 and stored in a gas-bottle prior to the experiments.

B. Experiments

Experiments were run at a 200 MHz NMR spectrometer (magnetic field $B_0 = 4.7$ Tesla) at 23° C. To observe the high-field SABRE effects we used a protocol (shown in Scheme 2) with the following stages: **Stage 1**: waiting period of a duration of τ_1 (usually 20 s) required for the spins to relax to thermal equilibrium at the field B_0. **Stage 2**: bubbling the H_2 gas enriched in its *para*-component (92 % *p*-H_2) through the solution. During this period the dihydrogen gas is efficiently dissolved in the sample. After the bubbling (duration 9.5 s) we stop the process and remove all remaining bubbles from the sample as it is important for the homogeneity of B_0. Altogether, the stage takes the time τ_b (here, 10 seconds). **Stage 3**: applying RF-irradiation for a variable time τ_{rf}, (varied in the range 0.1-7 s). **Stage 4**: detection of the transverse magnetization formed due to the high-field SABRE effect immediately after switching off the RF-field (i.e., without applying any detecting pulses). Total duration of the experiment is τ_e. The experiment can be repeated several hundreds of times for a single sample (see below). The duration of RF-excitation (the spin-locking period) is long enough that complex formation and dissociation can frequently occur; τ_{rf} is smaller than the relaxation time of the substrate protons. We checked that the polarization level gets saturated for our substrates at $\tau_{rf}\approx$5 s (while for the relaxation-based mechanism the saturation occurs only after about 100 s of bubbling[19]).

To bubble the sample by *p*-H_2 we used a thin plastic capillary that is inserted in the NMR tube allowing us to bubble the sample in the NMR spectrometer without loss of homogeneity. For stopping the bubbling we (1) close the *p*-H_2 source by a digitally controlled gas-valve and then (2) open another valve to ambient pressure to allow *p*-H_2 overpressure in the gas-line to vanish. The gas system used allows us to control the experiment by a computer and to start the NMR measurement 0.5 s after the stop of *p*-H_2 supply.

In order to optimize the polarization of dihydrogen, which has a shorter relaxation time than the substrates, it is required to use a short duration of the spin-locking period (τ_{rf}=0.7 s). When the RF-field amplitude ν_1 and frequency ν_{rf} are set properly (see Theory section), the substrate and dihydrogen acquire observable hyperpolarization. Transverse spin magnetization (free induction) is observable immediately after switching off the RF-field. By taking the Fourier transform of the free induction decay we obtained NMR spectra with enhanced lines. If instead of transverse magnetization longitudinal magnetization is desired it is simple to generate it by applying a proper pulse 90-degree out-of-phase with respect to the spin-locking RF-field.

Experiments were carried out at three different RF-field amplitudes equal to 28.6 kHz, 20.3 kHz and 11.4 kHz for the two Iridium complexes and Py as substrate. For the three other substrates we used the highest amplitude of ν_1=28.6 kHz. Here, only the parameters of the RF-field were optimized to get the highest enhancement factors but we did not optimize the concentration of substrates and iridium complexes nor the temperature to reach higher enhancement factors.

NMR enhancement factors were measured in the following way. Thermal polarization values were obtained from NMR spectra measured prior to bubbling the sample by *para*-H_2. Then the integrated lines of the substrate signals in RF-SABRE were divided by the corresponding thermal signals. To obtain the enhancement factor for dissolved dihydrogen and dihydride at the active complex we ran the SABRE experiments as described above; then, after a sufficiently long waiting period in order to let the spins relax to equilibrium we acquired a thermal NMR spectrum. After that, the enhancement factor for dihydrogen was obtained as the ratio of the integrated signals in the RF-SABRE spectrum and in the thermal NMR spectrum. The highest enhancement factors achieved for the substrate protons are shown in Chart 1.

Hereafter we also use the following abbreviations for different species: aPy and ePy for the axial and equatorial pyridine ligands, respectively, of the active complex; fPy for free pyridine in the solution; H_2 is dihydrogen in the solvent bulk, $c$$H_2$ is dihydride at the active complex.

III. Theory

A. Calculation method

To model the RF-SABRE hyperpolarization on the quantitative level we used a theoretical approach, similar to the one developed earlier[21]. We describe polarization transfer in a system, which consists of 2 spins originating from *para*-H_2 and N protons of the substrate: $N = 3$ for 2,2′-bipyrazine, $N = 4$ for 4,4′-bipyridine and $N = 5$ for pyridine and 3-methyl-1H-pyrazole. In the case of Crabtree's catalyst also the spin of the ^{31}P nucleus was included in the calculation. Thus, the total number of spins that we treat is $N + 2$ in case of IrIMes and $N + 3$ in case of Crabtree's catalyst. The spin system at high magnetic field, B_0, in the presence of the RF-field is described by the following Hamiltonian in the rotating reference frame:

$$\begin{aligned}\widehat{H}_{rf} = &-\sum_{\alpha=1}^{N+2}(\nu_\alpha - \nu_{rf})\hat{I}_{\alpha z} + \sum_{\alpha<\beta}^{N+2} J_{\alpha\beta}(\hat{\mathbf{I}}_\alpha \cdot \hat{\mathbf{I}}_\beta) - \nu_1 \sum_{\alpha=1}^{N+2} \hat{I}_{\alpha x} \\ &+ \left[-\nu_P \hat{F}_z + \sum_{\alpha=1}^{N+2} J_{\alpha P}\hat{I}_{\alpha z}\hat{F}_z\right]\end{aligned} \quad (1)$$

Here the spin operators of the α-th protons are denoted as $\hat{I}_{\alpha x,y,z}$; $\hat{F}_z$ defines the z-projection of the ^{31}P spin. The NMR frequencies of protons, ν_α, are given by their chemical shifts, δ_α, and the proton gyromagnetic ratio, γ: $\nu_\alpha = (1 + \delta_\alpha)\gamma B_0/2\pi$. The NMR frequency, ν_P, of the phosphorus nucleus is considerably different from those of the protons; for this reason only the z-operator of spin is important for ^{31}P. Proton-proton scalar couplings are denoted by $J_{\alpha\beta}$; proton-phosphorus couplings are denoted as $J_{\alpha P}$. To assign lines in the NMR spectra and

determine the NMR parameters we used high-resolution one-dimensional NMR spectra and two-dimensional TOCSY[24] spectra. All relevant NMR parameters, proton chemical shifts and J-couplings, are given in Tables 1S-5S for all systems under study in Supporting information (SI).

To describe the resulting spin order we calculated the density matrix of the spin system. As initial condition we have taken the density matrix, ρ_{in}, which describes the singlet-state preparation of the protons originating from *para*-H_2 and zero polarization for all the other spins. After that, this matrix was rewritten in the eigen-basis of the Hamiltonian $\widehat{H}_{rf}$; in this matrix we removed all off-diagonal elements and obtained the resulting density matrix, ρ_f. The removed elements describe spin coherences, which are washed out due to the long period of preparation of polarization. Then, using this new matrix, spin magnetizations, $M_{\alpha x}$ and $M_{\alpha y}$, were calculated as the expectation values of the corresponding spin operators:

$$M_{\alpha x} = \mathrm{Tr}\{\hat{I}_{\alpha x}\rho_f\}, \qquad M_{\alpha y} = \mathrm{Tr}\{\hat{I}_{\alpha y}\rho_f\} \tag{2}$$

This calculation scheme is known to be fast and precise to describe polarization transfer effects in PHIP and SABRE.[21, 25-26]

In the resulting dependences of RF-SABRE on the RF-field parameters, ν_{rf} and ν_1, in the case of multispin systems (e.g., protonated Py) noise-like contributions are seen, which arise from the large number of LACs in the coupled multi-spin system under study. Such noise-like features are irrelevant for the comparison with the experiment; furthermore, they disappear when inhomogeneity of the B_1-field is taken into account. For this reason, we performed calculations assuming a spatially non-uniform B_1-field, i.e., averaged the result over a realistic distribution over the ν_1 values. After this, the RF-SABRE dependences become smooth. Since signal amplitudes in the theory and in experiment are related arbitrarily, for a better comparison we also

normalized the theoretical curves to the corresponding experimental ones, keeping a common scaling factor for all protons in each substrate.

In this model we neglect the chemical exchange between bulk and bound substrate and between dihydrogen and dihydride during the spin-locking, neither do we take into account relaxation processes.

B. LACs in the doubly tilted frame

Let us now give our explanation of the SABRE mechanism and also discuss how the enhancement depends on the parameters of the RF-field. Here we do not go into full details of the spin dynamics, but provide a descriptive and reasonably simple treatment of the problem under study. Let us write down the Hamiltonian of the spin system under RF-excitation, see eqn. (1); however, for the sake of simplicity, we assume here that the substrate has only one spin (M-spin; $N = 1$) and that the chemical shifts of the protons coming from *para*-H_2 (AA′-protons) are identical (which is the case for both SABRE complexes with Py), i.e., the AA′-spins are 'isochronous'. This is the minimal spin system, in which the SABRE effect can be formed; it also corresponds to the previously studied case of deuterated Py having only one ortho-proton[4]. Then the Hamiltonian in the rotating frame is:

$$\begin{aligned}\widehat{H}_{rf}^{AA'M} = &-\delta\nu_A\left(\hat{I}_{Az} + \hat{I}_{A'z}\right) - \delta\nu_M\hat{I}_{Mz} + J_{AA'}\left(\hat{\mathbf{I}}_A \cdot \hat{\mathbf{I}}_{A'}\right) \\ &+ \left[J_{AM}\left(\hat{\mathbf{I}}_A \cdot \hat{\mathbf{I}}_M\right) + J_{A'M}\left(\hat{\mathbf{I}}_{A'} \cdot \hat{\mathbf{I}}_M\right)\right] - \nu_1\left(\hat{I}_{Ax} + \hat{I}_{A'x} + \hat{I}_{Mx}\right)\end{aligned} \tag{3}$$

where $\delta\nu_\alpha = \left(\nu_\alpha - \nu_{rf}\right)$; $J_{\alpha\beta}$ are the scalar spin-spin interaction constants. Here it is convenient to treat the following terms

$$\hat{V} = J_{AM}\left(\hat{\mathbf{I}}_A \cdot \hat{\mathbf{I}}_M\right) + J_{A'M}\left(\hat{\mathbf{I}}_{A'} \cdot \hat{\mathbf{I}}_M\right) \tag{4}$$

as a small perturbation. This is a good approximation when $J_{AA'}$ is by far the largest coupling in the spin system (which is true in the case of SABRE). The main part of the Hamiltonian, $\widehat{H}_0 = \widehat{H}_{rf}^{AA'M} - \widehat{V}$, can be most conveniently written in the so-called Doubly Tilted Frame (DTF) where the spins in each group (AA′-protons and M-proton) are quantized along their own effective fields in the rotating frame, see Figure 1a. In this frame $\widehat{H}_0$ takes the form:

$$\widehat{H}_{0,dtf} = -\nu_{A,dtf}\left(\hat{I}_{Az} + \hat{I}_{A'z}\right) - \nu_{M,dtf}\hat{I}_{Mz} + J_{AA'}\left(\hat{\mathbf{I}}_A \cdot \hat{\mathbf{I}}_{A'}\right) \tag{5}$$

where $\nu_{A,dtf} = \sqrt{(\delta\nu_A)^2 + \nu_1^2}$ and $\nu_{M,dtf} = \sqrt{(\delta\nu_M)^2 + \nu_1^2}$. Transition to the DTF does not affect couplings between 'isochronous' spins of one group (here it is $J_{AA'}$) and changes coupling between others protons, see below. In the DTF there are two level crossings occurring when

$$\nu_{A,dtf} - \nu_{M,dtf} = \pm J_{AA'} \tag{6}$$

These crossings are between the energy levels corresponding to the state composed of the singlet configuration of the AA′-protons and β of the M-proton, $|S\beta\rangle$, and of the lower triplet state of the AA′-protons and α of the M-proton, $|T_-\alpha\rangle$, in the DTF (corresponding to the "+" sign in eqn. (6)) or between $|S\alpha\rangle$ and the upper triplet state of the AA′-protons and β of the M-proton, $|T_+\beta\rangle$ (corresponding to the "–" sign in eqn. (6)); initially only the levels with singlet character of the AA′-spins are populated. At the level crossing points the perturbation term $\widehat{V}$ becomes important: when AA′ are magnetically nonequivalent, i.e., when $J_{AM} \neq J_{A'M}$, it mixes the states and turns the crossing into an LAC. Consequently, the populations of the involved levels are mixed. When the system is brought to the LAC between the $|S\beta\rangle$ and $|T_-\alpha\rangle$ states, see Figure 1b, this kind of mixing results in negative polarization of the AA′-spins along their effective field in the DTF and positive polarization of the M-spin along its effective field in the DTF. For the other LAC between states $|S\alpha\rangle$ and $|T_+\beta\rangle$ (Figure 1c) the resulting polarization is of the same size, but

opposite sign for both the AA′ and M-protons. The full ν_{rf} dependence of polarization is schematically shown in Figure 1f. This simple model leads to two important consequences: (i) the RF-frequency dependence of polarization is anti-symmetric with respect to the center of the spectrum, $(\nu_A + \nu_M)/2$; (ii) polarization of the AA′-protons (H_2) has opposite sign to that of the M-proton belonging to the substrate.

Finally, let us discuss the conditions for having an LAC in the DTF. From eqn. (6) it follows that the two frequencies, $\nu_{A,dtf}$ and $\nu_{M,dtf}$, have a difference equal to $\pm J_{AA'}$, which is achieved when the frequency ν_{rf} is placed almost at the center of a spectrum, $(\nu_A + \nu_M)/2$, having only a small offset from this value (either positive or negative). In addition, to make the mixing of states efficient it is required that the angle between the two quantization axes of the DTF, $\Theta = \theta_A + \theta_M$, significantly deviates from π, see Figure 1a. This is because the terms describing coupling between different groups of 'isochronous' spins is modified upon going to DTF. The reason for this is that the quantization axes are different for different groups of spins; consequently, the perturbation, $\hat{V}$, must be written as follows[21]:

$$\hat{V}_{dtf} = \frac{\cos^2\Theta/2}{2} J_{AM}\left(\hat{I}_{A+}\hat{I}_{M-} + \hat{I}_{A-}\hat{I}_{M+}\right) + \frac{\cos^2\Theta/2}{2} J_{A'M}\left(\hat{I}_{A'+}\hat{I}_{M-} + \hat{I}_{A'-}\hat{I}_{M+}\right) + \text{additional terms} \tag{7}$$

Here we show only the elements of $\hat{V}_{dtf}$ that cause flip-flop transitions. Consequently, the matrix element, which mixes the crossing state, for instance, $|S\beta\rangle$ and $|T_-\alpha\rangle$ is proportional to the following quantity[21]:

$$\left(J_{AM} - J_{A'M}\right)\cos^2\Theta/2 \tag{8}$$

Thus, to enable flip-flop transitions between the spins from different groups it is necessary that Θ significantly deviates from π. In turn, this condition is achieved when ν_1 is sufficiently large, i.e.,

it is larger than or at least comparable to $(\nu_A - \nu_M)$. In this situation in the course of mixing at the LAC regions the spins acquire magnetization along the x-axis in the non-tilted rotating frame, which is detected in our experiments. This is important because here we do not use any additional read-pulses but start to acquire the x-magnetization, M_x, that is generated during the spin mixing, immediately after switching off of RF-pulse.

We have discussed the positions of LACs in the simplest system of an AA′M-type that is indeed the minimal system, which can be treated in the context of SABRE. However, there is still the question whether the results for the AA′M-system also apply to systems with more coupled protons. To answer this question, let us analyze the LACs in the case where the substrate has two 'isochronous' protons, so that the resulting spin system is of the AA′MM′-kind. We also assume that there are two strong couplings in the system, the AA′ and MM′-coupling (at least one of them should be strong) while the remaining couplings are significantly smaller. In this situation the AA′- and MM′-couplings can be included in the main Hamiltonian, whereas the four AM-couplings are treated as a perturbative part, $\hat{V}$. This allows us to write down the positions of LACs in the DTF [20-21]:

$$\begin{aligned} \pm\left(\nu_{A,dtf} - \nu_{M,dtf}\right) &= J_{AA'} - J_{MM'};\ |ST_{\pm}\rangle_{dtf} - |T_{\pm}S\rangle_{dtf} \text{ level crossings} \\ \pm\left(\nu_{A,dtf} - \nu_{M,dtf}\right) &= J_{AA'} + J_{MM'};\ |SS\rangle_{dtf} - |T_{\pm}T_{\mp}\rangle_{dtf} \text{ level crossings} \end{aligned} \tag{9}$$

Thus, it is seen that the number of LACs has doubled as compared to the AA′M case. However, when $J_{AA'} \gg J_{MM'}$ the LACs are grouped in two pairs with almost the same positions (it is the case of two ortho-protons of Py in the IrIMes complex). Hence, each pair of LACs, (i) $|ST_+\rangle_{dtf} - |T_+S\rangle_{dtf}$ and $|SS\rangle_{dtf} - |T_+T_-\rangle_{dtf}$, (ii) $|ST_-\rangle_{dtf} - |T_-S\rangle_{dtf}$ and $|SS\rangle_{dtf} - |T_-T_+\rangle_{dtf}$, works as a single LAC because both of them lead to polarization of the same kind. It is typical, that the AA′-coupling is the largest (about –7 Hz), whereas the coupling between the protons of

the substrate is smaller; for instance, between the two ortho-protons of Py it is below 1 Hz. For this reason, the relatively simple three-spin model of the four spin system gives already a valid quantitative description of the problem. When there are more spins in the system and the relation between them is arbitrary the LACs can only be identified from precise quantum-mechanical calculations: This is exactly the approach that we used to model the data. Nonetheless, the description presented above gives a short-cut to an appropriate quantitative understanding of the problem under consideration; in many cases, the positions of LACs can be determined using eqns. (6) and (9).

IV. Results and discussion

Here we discuss the details of the dependence of the RF-SABRE effect on the two key parameters, RF-frequency ν_{rf} and RF-amplitude ν_1. We present the results for 2,2′-bipyrazine, 4,4′-bipyridine 3-methyl-1*H*-pyrazole and Py with the IrIMes complex and Py with Crabtree's catalyst (see Chart 1 and Scheme 1). Polarization of the substrate protons and polarization of the dihydrogen in the bulk solution (H_2) and of the dihydride in the active complex (cH_2) is also discussed. As an example the structure of the active complex for L=IMes with Py, as well as the reaction pathway leading to the SABRE effect are shown in Scheme 1. In Scheme 1 it is indicated that polarization from cH_2 is transferred only to the equatorial Py ligands. While this applies to IrIMes, one can in the case of Crabtree's catalyst transfer polarization to the axial ligand too (compare the results for Py with the two iridium complexes). The reaction scheme is similar for the other substrates under study, which undergo exchange between two states, the catalyst-bound ligands and the free substrate in bulk solution.

2,2′-bipyrazine with IrIMes. The highest enhancement factor for RF-SABRE among the substrates that are presented here is found for 2,2′-bipyrazine, being about 200-300 for the H3

proton, (see spectra in Figure 2). Spectra 1 and 2 in Figure 2 are taken when the LAC conditions are exactly fulfilled for the three-spin system of $c\mathrm{H}_2$ and the H3 proton; however, one should note that in spectrum 2 there is also negative polarization on the H5 and H6 protons formed at the LACs in the four-spin subsystem ($c\mathrm{H}_2$, H5 and H6). For the sake of simplicity, here coupling between the H3 proton and the H5 and H6 protons is neglected. This is a valid description because the chemical shift difference at 4.7 T between the H3 protons and the H5, H6 protons is about 150 Hz, whereas the J-coupling is only 1.2 Hz. However, the coupling between the H5 and H6 protons cannot be neglected, since the chemical shift difference is only about 20 Hz. The experimental results are consistent with this assumption: the RF-SABRE frequency dependences are different for the H3 proton and for the H5, H6 protons; for each group of protons there is a positive and a negative component in the ν_{rf} dependence. The frequency dependence for $c\mathrm{H}_2$ and H_2 is a superposition of the two components: dihydride is polarized in the three-spin subsystem ($c\mathrm{H}_2$ and H3) and in the four-spin subsystem ($c\mathrm{H}_2$, H5 and H5). This separation of the spin system helps to make the qualitative description simpler; while numerical calculation was done for the entire five-spin system strongly supporting the qualitative arguments: as it is seen from Figure 2 the experimental frequency dependences are in good agreement with the calculation. The RF-frequency ν_{rf} is chosen such (in case of spectra 1 and 2) that it is placed almost at the 'center of the spectrum', that is, at $\nu_{rf} = (\nu_{c\mathrm{H}_2} + \nu_M)/2$, (here ν_M stands for the NMR frequency of the proton of bipyrazine in the active SABRE complex) but, in accordance with eqns. (6) and (9), slightly detuned from this value. Positive and negative frequency offsets result in different sign of polarization of the H3 proton, which is always opposite to polarization of $c\mathrm{H}_2$ and H_2, in full accordance with our theoretical treatment. When the RF-frequency is such that the system stays away from any LAC the RF-SABRE effect vanishes: in spectrum 3 there is

no polarization of the H3 proton (there is no LAC for the three-spin subsystem), while the H5 and H6 protons are polarized as the LAC conditions for the four-spin subsystem are fulfilled.

4,4′-bipyridine with IrIMes. Likewise, for 4,4′-bipyridine positive or negative RF-SABRE enhancement can be observed by varying the RF-frequency, see Figure 3. The maximal achieved enhancement is 13 for the H2,2′ and H6,6′ protons. Results obtained for 4,4′-bipyridine illustrate an important detail of the RF-SABRE method. In spectra 1 and 2 in Figure 3 enhancements are seen for the H2,6 protons in free bipyridine and in bipyridine bound to the SABRE complex (*c*H2,6). In order to match the LAC condition and to generate RF-SABRE one has to place the RF-frequency almost at the center between the NMR lines of cH_2 and *c*H2,6 (but not of H2,6) see eqns. (6) and (9); subsequently, the H2,6 protons acquire hyperpolarization due to chemical exchange of the substrate (see Scheme 1). The frequency dependence has the characteristic bimodal shape for both groups of the substrate protons (see Figure 3); polarization for both forms of H_2 always has the phase opposite to that of the substrates. Interestingly, in 4,4′-bipyridine one can also split the entire spin system into two four-spin subsystems: cH_2 coupled to the H2,6 protons and cH_2 coupled to the H3,4 protons. In each subsystem, the frequency dependence of dihydrogen is always a mirror image of that for the substrate and the total RF-SABRE effect for cH_2 and H_2 is a superposition of the dependences for the two subsystems.

3-methyl-1H-pyrazole with IrIMes. The RF-SABRE spectra for 3-methyl-1H-pyrazole for different RF-frequencies are given in Figure 4. A signal enhancement of about 40 is achievable for this substrate. 3-methyl-1H-pyrazole is a good example demonstrating the bimodal RF-SABRE frequency dependence (see Figure 4). As in the previous cases, we can split the full spin system into three individual subsystems because the CH_3, H4 and H5 protons relatively weakly interact with each other. A theoretical estimate shows that for the B_0 field strength and RF-field

strength used, LACs in individual subsystems with $c\mathrm{H_2}$ are well-separated from each other. As a result, the frequency dependence of RF-SABRE (Figure 4) has three pairs of dips and peaks for the $c\mathrm{H_2}$ and $\mathrm{H_2}$ protons that correspond to LACs in ($c\mathrm{H_2}$, H5), ($c\mathrm{H_2}$, H4) and ($c\mathrm{H_2}$, $\mathrm{CH_3}$) subsystems. As previously, the polarization of dihydrogen and dihydride on the one hand and the substrate protons on the other hand is always opposite in sign.

Pyridine with IrIMes. Now let us describe the results for RF-SABRE of Py, which is currently the most common substrate in SABRE experiments. Typical RF-SABRE spectra of Py with IrIMes are shown in Figure 5: one can readily see that for obtaining the effect it is crucial to set carefully the RF-field frequency.

Complete frequency dependences for all Py protons, dihydride and dihydrogen are shown in Figure 5. The highest enhancement is observed for the *ortho*-protons of Py, Py-*o*; while all other protons (namely, the *meta*-protons of Py denoted as Py-*m*, $\mathrm{H_2}$ and $c\mathrm{H_2}$) are polarized much weaker.

The frequency dependences of RF-SABRE at any ν_{rf} are in very good agreement with our calculations; and the opposite phase of $\mathrm{H_2}$ and $c\mathrm{H_2}$ compared to the *ortho*-protons of Py additionally supports our theoretical predictions. It is known that Py in the IrIMes complex has two different positions[9]: equatorial (ePy) and axial (aPy). As follows from our experiments, mainly ePy exchanges with free Py in the solution. Therefore one has to set ν_{rf} at the center between $c\mathrm{H_2}$ and one of the Py protons in the complex to obtain polarization of the corresponding Py species. We tried to transfer polarization to both ePy and aPy but achieved significant spin order transfer only to ePy. The reason why polarization can be transferred directly to ePy, but not to aPy is, most probably, because the J-couplings between $c\mathrm{H_2}$ and

protons of ePy are considerably stronger than those between *c*H_2 and aPy, a requisite that is essential for efficient polarization transfer. Because polarization is transferred to ePy that exchanges with free Py strong polarization on free Py is observed (see Figure 5). For calculation we used the NMR parameters of the 7-spin system describing *c*H_2 coupled to ePy.

For all substrates the achieved signal enhancement is high, but still smaller than that found for the SABRE effect at low fields[8, 10, 18]. We attribute this decrease of polarization as compared to the low-field case to association-dissociation processes occurring during the spin-locking period. Since the chemical shifts of all protons are different at the complex and in the solution these chemical exchange processes result in modulation of $\nu_{A,dtf}$ and $\nu_{M,dtf}$ and also of the direction of the tilted axes. This causes variation of the RF-irradiation conditions, which tends to reduce polarization. When SABRE is done at low field this effect is not pronounced because all spins are then quantized along a fixed axis given by the direction of the external magnetic field. To reduce the unwanted effect at high field it is desirable to use strong RF-fields such that the DTF quantization axes almost coincide with the x-axis of the rotating frame for both free and catalyst-bound substrate. Our results clearly show that when ν_1 increases polarization grows in accordance with this expectation, see Figure 1S of SI, and coincides with similar observations[20-21]; however, with the field strengths available we were unable to reach the condition $\nu_1 \gg |\delta\nu_A|, |\delta\nu_M|$. Polarization of H_2 should be even more sensitive to the modulation effect because of the very large difference in the chemical shift of H_2 bound to catalyst (–22.8 ppm) and H_2 in solution (4.6 ppm). For this reason, and also because of fast relaxation of H_2 and the fact that some amount of H_2 goes to the gas phase, the absolute signal intensity for H_2 is much smaller than for the Py protons but is still substantial.

For Py the relaxation time is longer and the difference in chemical shift between the free and bound states is smaller than that for H_2 and cH_2, therefore high absolute signal intensities are achievable. Hence, the duration of RF-field, τ_{rf}, when cH_2 polarization reaches saturation (about 0.7 s) is significantly shorter than for Py (about 5 s).

Pyridine with Crabtree's catalyst. Finally, let us present the results for Py with Crabtree's catalyst, which is known to be another efficient SABRE catalyst. Experiments were done in the same fashion as for the IrIMes catalyst; again, the SABRE effect is due to spin mixing at LACs in the DTF, as follows from the RF-frequency dependence of polarization. The resulting spectra are shown in Figure 6.

The frequency dependences for RF-SABRE of the Py-*o* at three different amplitudes of RF-field ν_1 are shown in Figure 7. Of all Py protons Py-*o* acquire the highest NMR enhancement. In all cases the dependence has a positive and a negative component, due to specific LACs in the DTF. As for the IrIMes case, our theoretical treatment reproduces well the experimentally observed dependences. The results also demonstrate that sufficiently high ν_1 values are required to provide a considerable high-field SABRE effect. In contrast to IrIMes, for Crabtree's catalyst the polarization transfer proceeds from cH_2 to both, ePy and aPy. It can be seen from comparison of the ν_{rf}-dependences of the Py-*o* with IrIMes (Figures 1S (SI) and 5) and with Crabtree's catalyst (Figure 7). In the case of IrIMes the frequency dependences are symmetric and (as we mentioned above) polarization is transferred mainly to ePy. In the case of Crabtree's catalyst the frequency dependences are not symmetric. For this reason, we suggest that polarization is transferred to both ePy and aPy; to confirm this assumption we calculated the substrate polarization for both channels of spin order transfer, namely for both 8-spin systems of the complexes with Crabtree's

catalyst. The resulting frequency dependences were summed with different weights. Taking into account the contributions from both systems is required to model the experimental curves. The results presented in Figure 7 show that polarization transfer to aPy and ePy is comparable only at low v_1, whereas at high v_1 polarization is mainly transferred to ePy.

Figure 8 presents the results for *c*H_2 and H_2. Here the frequency dependences have opposite sign as compared to Py-*o* (see Figure 7). Again, to explain the frequency dependences it is necessary to take into account both transfer channels with aPy and with ePy. However, it is not yet clear why the polarization dependences for *c*H_2 and H_2 are different because one would expect that they are identical as in case of IrIMes (see Figure 5). The simulation curves for *c*H_2 and H_2 are sums of those for the two channels with aPy and with ePy; the scaling factors, however, are different for *c*H_2 and H_2. As it is seen from the experimental curves *c*H_2 behaves here more like *c*H_2 in the complex with ePy and H_2 more like *c*H_2 in the complex with aPy.

In general, for all the protons under study the experimental results are in good agreement with the simulation. The characteristic dependence of the polarization amplitude and its sign on the RF-frequency shows that the reported high-field SABRE effect is based on LACs, which enable efficient and fast transfer of spin order from parahydrogen to the substrate.

Re-hyperpolarization experiments at high field. Now let us demonstrate a further advantage of the RF-SABRE method, namely the possibility to repeatedly re-hyperpolarize the nuclear spins. For this purpose, we slightly modified the experimental protocol shown in Scheme 2: frequency, amplitude and duration of the RF-irradiation at stage 3 are now kept fixed (τ_b=10 s, τ_{rf}=0.4 s), while the waiting time τ_1 (stage 1) was used as variable parameter. We continuously repeated the experiments while reducing τ_1 and thus τ_e after 20 each repetitions. The results are

presented in Figure 9. It is readily seen that for the same total experimental time τ_e the enhancement stays on the same level; continuous measurements do not reveal any loss of enhancement for at least several hundreds of experiments. In particular the absence of any decrease in polarization allowed us to measure the frequency dependences shown in this work using only a single sample for each system. Interestingly, when the experimental timing is reduced the signal enhancement only grows, from 200 to 300 for 2,2′-bipyrazine. We attribute this growth to the following factor: as our RF-amplitude ν_1 is rather low and $\nu_1 \gg |\delta\nu_A|, |\delta\nu_M|$ is not fulfilled, spin nutation is occurring not in the xy-plane, but on a cone around the effective magnetic field in the rotating frame; hence, the magnetization acquires a z-component, which does not decay, when the RF is switched off, but stays for a time T_1. When the RF is switched on again, the remaining z-component takes again part in the nutation and thus increases the observed x-component. Therefore we achieved a higher enhancement factor when τ_1 and thus τ_e was reduced. For the same reason we expect even higher enhancement factors when ν_1 is increased.

V. Conclusion and outlook

To summarize, we demonstrated and analyzed a method to perform ^{1}H SABRE experiments (RF-SABRE) at high magnetic field. The RF-SABRE signal enhancements achieved are summarized in Chart 1. It is seen that the effect is not limited to the most common SABRE substrate Py but is clearly more general. Using the same approach as in our recent work[4], it is possible to polarize other molecules containing a nitrogen atom in the aromatic ring. For 2,2′-bipyrazine an NMR enhancement of about 200-300 is achieved. In other cases the NMR enhancement is lower but still significantly larger than that given by the cross-relaxation mechanism. Thus, despite the more complex spin dynamics in systems with several protons (in

comparison with the three-spin system of partially deuterated Py[4]), it is feasible to achieve a significant RF-SABRE effect. Its dependence on the key experimental parameters, amplitude, frequency, and duration of RF-irradiation, is explored; different channels of chemical exchange are separated.

The RF-SABRE method exploits mixing of spin states at LACs; the LAC conditions are fulfilled by turning on a strong RF-field with properly chosen amplitude and frequency. Optimization of RF-field parameters enables implementing the low-field conditions, that is, the LACs, staying at a high magnetic field and opening efficient pathways for coherent transfer of hyperpolarization. Thus, the LACs are the key element of the RF-SABRE method. By varying the RF frequency one can also vary the phase of polarized NMR signals in a simple and desirable way. These results can be well described by the theoretical treatment presented here; also a simple semi-qualitative explanation of our observations is given here that is based on spin mixing and LACs in the doubly tilted frame of reference.

The signal enhancements obtained here are significant but still lower than those obtained in SABRE experiments in a low static field. For instance, Dücker et al.[8] have obtained signal enhancements of the order of 1,000 for the *ortho*-protons of Py and of the order of 200 for different pyrazole derivatives at conditions, similar to those used in our work. We attribute the decrease of the enhancement in RF-SABRE to stochastic modulation of the effective field experienced by spins in the rotating frame, leading to the reduction of polarization. Such a problem is absent in low-field experiments because spins acquire polarization with respect to the time-independent static magnetic field. Comparing low-field SABRE and RF-SABRE it is also important to emphasize that individual protons are polarized in a different way in these two experiments. At low fields, polarization is predominantly transferred from *p*-H_2 to the protons

having the strongest $J_{AM}, J_{A'M}$ couplings; subsequently, polarization is transferred over the substrate molecule[11]. This is because of 'strong coupling' of the entire spin system at low fields: when the difference in the Zeeman interactions of spins with the external field is smaller than or comparable to their coupling a coherent polarization transfer mechanism becomes operative[5] and polarization is spread over a substrate molecule. In contrast, in RF-SABRE substrate protons are usually polarized individually at corresponding LACs: these LACs are occurring at distinct and different ν_{rf} frequencies, furthermore, at each LAC the substrate protons are only weakly coupled to each other. Thus, in RF-SABRE the protons acquire polarization via direct spin order transfer from the *c*H_2 protons in the SABRE complex; the transfer efficiency thus corresponds to the J-coupling strength between the corresponding protons and *c*H_2.

With the signal enhancement reaching 200-300 for substrate protons and 600 for dihydride in the active complex, our method is a significant step forward for establishing SABRE as a high-field technique. The method is relatively straightforward in use and only requires careful setting of the RF-field parameters. Since carrying out experiments at high magnetic fields is technically much easier as it avoids field-cycling and requires only standard NMR equipment we anticipate that our method will give access to exciting applications in NMR spectroscopy and imaging providing a permanent source of nuclear hyperpolarization. Recently, Theis et al. have demonstrated a high-field SABRE technique (LIGHT-SABRE)[3] that uses another group of LACs and allows one to transfer polarization from the *c*H_2 protons to heteronuclei, namely, to ^{15}N. Development of high-field SABRE methods will open new avenues in NMR and MRI using hyperpolarized nuclear spins.

An important development is the possibility of re-hyperpolarizing the spins in RF-SABRE experiment, as shown here: within only 10 seconds one can obtain the RF-SABRE spectrum

again and the signal enhancement stays the same for several hundreds of successive measurements. Thus, RF-SABRE enables a permanent source of hyperpolarization in NMR and MRI directly at a high magnetic field where the NMR spectral resolution is maximized. This is in contrast to some of the hyperpolarization techniques. For instance, the dissolution DNP technique, which provides a tremendous NMR signal enhancement of about 10,000, is limited to single-shot experiments[27]. The same holds for spin-hyperpolarized noble gases[28-29] despite spin polarization of the order of percent or tens percent one can use a batch of polarized spins only once. The standard PHIP method[17] suffers from a problem that the substrate is chemically modified: after saturation of C-C bonds it does not interact with parahydrogen any further. The CIDNP technique[30] usually suffers from depletion of the chemical system, in which hyperpolarization is produced: like the classical PHIP after certain number of acquisitions the system cannot be polarized anymore. An example of a liquid-state hyperpolarization technique, which enables re-polarization is the Overhauser-DNP: this method is operative at high field providing NMR enhancements of the order of 100[31-33], which is sustainable in repetitive experiments. While DNP is usually a more universal technique, RF-SABRE can be advantageous for several reasons: (i) signal enhancement is higher; (ii) there are no paramagnetic substances in the solution, which shorten the nuclear relaxation times and reduce spectral resolution; (iii) NMR samples of standard size can be used; (iv) problems associated with high-frequency microwave pumping are avoided. Thus, the feasibility of high-field ^{1}H SABRE experiments opens new avenues in exploiting hyperpolarized spins in NMR spectroscopy and imaging.

ASSOCIATED CONTENT

Supporting Information contains the ν_1 dependence of the RF-SABRE effect and NMR parameters of the SABRE complexes used in this work. This material is available free of charge via the Internet at http://pubs.acs.org.

AUTHOR INFORMATION

Corresponding Authors

Andrey N. Pravdivtsev, tel. +7(383)333-1333, fax +7(383)333-1399, e-mail: a.n.true@tomo.nsc.ru

Konstantin L. Ivanov, tel. +7(383)330-8868, fax +7(383)333-1399, e-mail: ivanov@tomo.nsc.ru

Author Contributions

The manuscript was written through contributions of all authors. All authors have given approval to the final version of the manuscript.

Funding Sources

This work was supported by the Russian Science Foundation (grant No. 14-13-01053). H.M.V. acknowledges the Alexander von Humboldt Foundation.

ACKNOWLEDGMENT

We are thankful to Dr. Pavel Petrov for providing us with the IrIMesCODCl pre-catalyst.

ABBREVIATIONS

DTF = Doubly Tilted Frame, LAC = Level Anti-Crossing, NMR = Nuclear Magnetic Resonance, Py = pyridine, RF = Radio-Frequency, SABRE = Signal Amplification By Reversible Exchange, TOCSY = total correlation spectroscopy

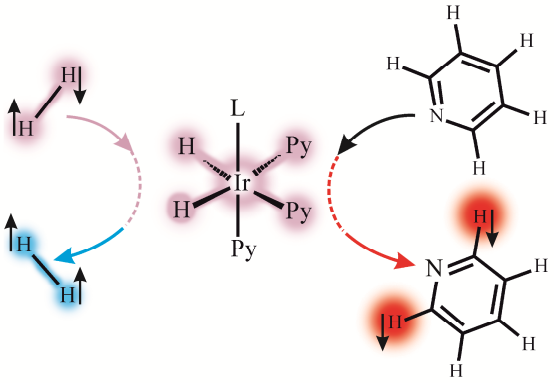

Scheme 1. SABRE formation in the complex of the Ir based catalyst with parahydrogen and pyridine (Py); Here L=IMes (1,3-bis(2,4,6-trimethylphenyl imidazole-2-ylidene)) or L=PCy_3 (tricyclohexyl phosphine). Transfer of the initial singlet spin order (represented by two anti-parallel arrows) of the parahydrogen molecule entering the complex results in polarization of Py (represented by "down" arrows near the ortho protons); at the same time, the H_2 molecule goes to its ortho-state (shown by "up" arrows). Here, for simplicity, polarization transfer to the equatorial Py and exchange of the equatorial Py with free Py in solution are schematically depicted; in real SABRE complexes the axial Py ligand is also involved in polarization transfer and SABRE formation.

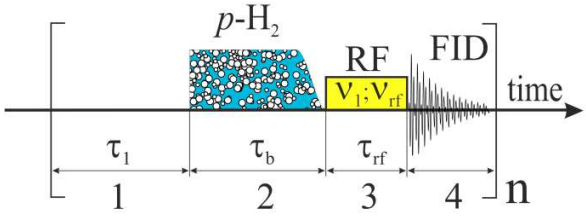

Scheme 2. The scheme of continuous RF-SABRE experiment is presented: (stage 1) waiting during the time τ_1 to allow all hyperpolarization that remain from the previous RF-SABRE cycle to relax; (stage 2) bubbling by p-H_2 during the time period τ_b; (stage 3) application RF-pulse with amplitude v_1 and frequency v_{rf} during the time period τ_{rf}; (stage 4) measuring the Free Induction Decay (FID). Total time of one RF-SABRE experiment is τ_e. The experiment can be repeated several hundreds of times for the single sample.

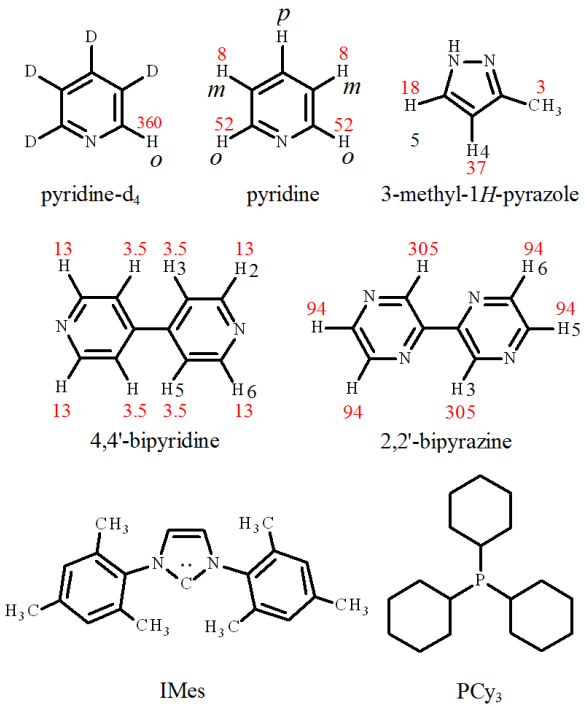

Chart 1. Chemical structures of substrates used; assignments of the proton positions and absolute values of the achieved NMR signal enhancements in comparison with NMR signal at 4.7 Tesla are also specified. Structure of pre-catalyst ligands, IMes and PCy_3, is also shown.

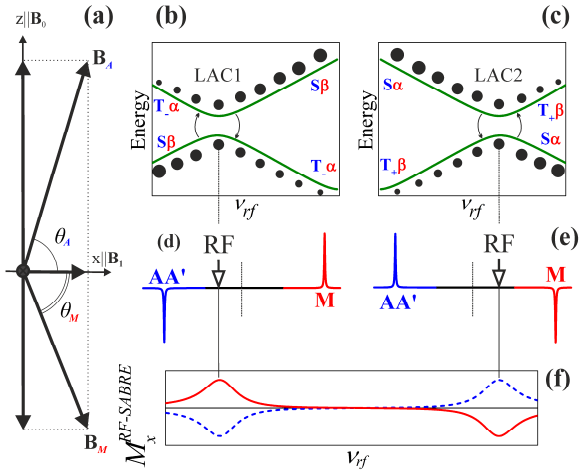

Figure 1. Schematic representation of the axes of the doubly tilted frame (DTF) (a) for three spin system AA′M: spins are quantized along the new axes, $\mathbf{B}_A$ and $\mathbf{B}_M$; they are inclined with respect to the x-axis, the inclination angles being θ_A and θ_M. In (b) and (c) we show the LACs in the DTF between the levels $|S\beta\rangle$ and $|T_-\alpha\rangle$ (LAC1) and between the levels $|S\alpha\rangle$ and $|T_+\beta\rangle$ (LAC2). Arrows represent transfer of polarization between two states at LAC region. In (d) and (e) the NMR spectra resulting from spin mixing at each LAC (with the position of the applied RF-field indicated by an arrows) shown under the corresponding energy diagram. Subplot (f) schematically shows polarization of the AA′-spins (dashed line) and M-spin (solid line) as a function of ν_{rf}. In (b) and (c) the size of balls represents populations of the spin levels after spin mixing under the action of RF-excitation in the case where the AA′ protons are born in the singlet state and other spins are not polarized.

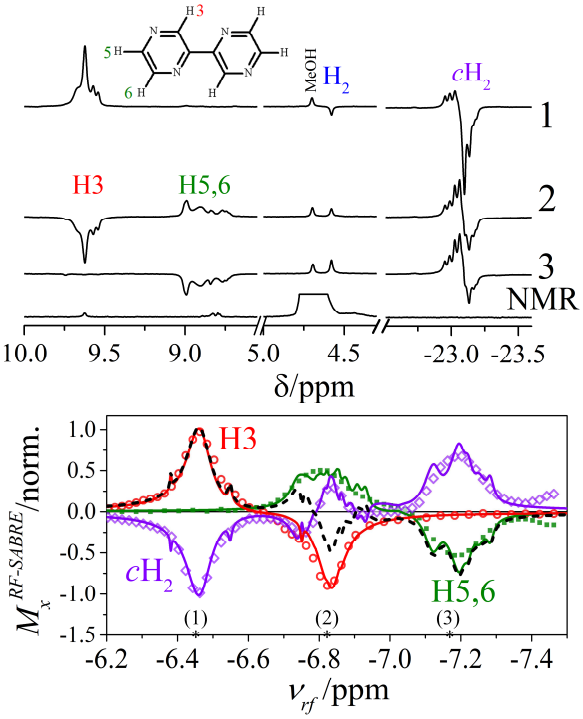

Figure 2. (top) ^{1}H RF-SABRE spectra of 2,2′-bipyrazine with the IrIMes in mixture of 80% methanol and 20% DMSO obtained after applying an RF-field with amplitude of 28.6 kHz and frequency positions at –6.46 ppm (trace 1), –6.84 ppm (trace 2) and –7.18 ppm (trace 3). The thermal single-scan NMR spectrum is also shown for comparison (bottom trace). Positions of different protons are assigned. (bottom) Dependence of the RF-SABRE effect on ν_{rf} is shown; asterisks denote ν_{rf} positions, for which RF-SABRE spectra (top) have been obtained. Here ν_1=28.6 kHz, τ_{rf}=0.4 s, τ_1=20 s, τ_e=35 s. cH$_2$ is the dihydrogen at the active complex. Lines are result of computation with the NMR parameters listed in the Table 1S (SI); dashed line shows the calculated polarization of all protons of the substrate. Maximal enhancement factors $\varepsilon = M_x^{RF-SABRE}/M_z^{thermal}(B_0 = 4.7\ T)$ are 194 for H3, 60 for H5 and H6 and 700 for cH$_2$.

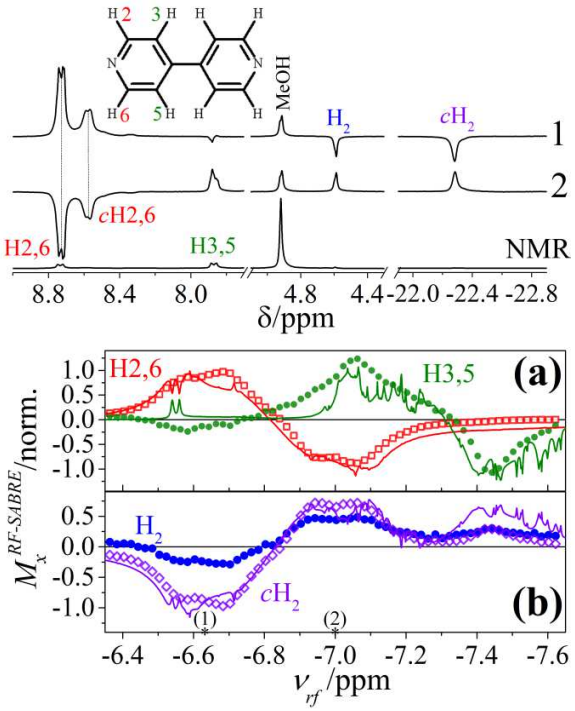

Figure 3. (top) 1H RF-SABRE spectra of 4,4′-biryridine with the IrIMes in methanol obtained after applying an RF-field with amplitude of 28.6 kHz and frequency positions at –6.6 ppm (trace 1) and –7. 60 ppm (trace 2). The thermal single-scan NMR spectrum is also shown for comparison (bottom trace). Positions of different protons are assigned. (bottom) Dependence of the RF-SABRE effect on ν_{rf} is shown; asterisks denote ν_{rf} positions, for which RF-SABRE spectra (top) have been obtained. In (a) the results are shown for the substrate protons and in (b) the results are shown for H_2 and cH$_2$. Here ν_1=28.6 kHz, τ_1=20 s; in (a) τ_{rf}=10 s in (b) τ_{rf}=0.6 s. Lines are result of computation with the NMR parameters listed in the Table 2S (SI). Maximal enhancement factors $\varepsilon = M_x^{RF-SABRE}/M_z^{thermal}(B_0 = 4.7\ T)$ are 13 for H2,6, 3.5 for H3,5, 40 for H_2 and 80 for cH$_2$.

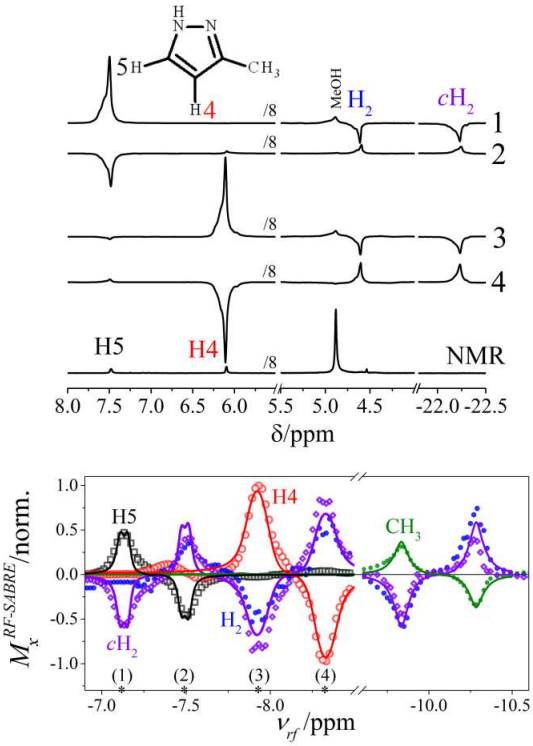

Figure 4. (top) ^{1}H RF-SABRE spectra of 3-methyl-1H-pyrazole with the IrIMes in methanol obtained after applying an RF-field with amplitude of 28.6 kHz and frequency positions at – 8.33 ppm (trace 1), –7.93 ppm (trace 2), –7.5 ppm (trace 3) and –7.13 ppm (trace 4). The thermal single-scan NMR spectrum is also shown for comparison (bottom trace). Positions of different protons are assigned. (bottom) Dependence of the RF-SABRE effect on ν_{rf} is shown; asterisks denote ν_{rf} positions, for which RF-SABRE spectra (top) have been obtained. In (a) the results are shown for the substrate protons and in (b) for H_2 and cH$_2$ and the methyl group of the substrate. Here ν_1=28.6 kHz, τ_1=20 s; in (a) τ_{rf}=7 s in (b) τ_{rf}=2.2 s. Lines are result of computation with the NMR parameters listed in the Table 3S (SI). Maximal enhancement factors $\varepsilon = M_x^{RF-SABRE}/M_z^{thermal}(B_0 = 4.7\ T)$ are 18 for H5, 37 for H4, 3 for CH_3-group, 15 for H_2 and 20 for cH$_2$.

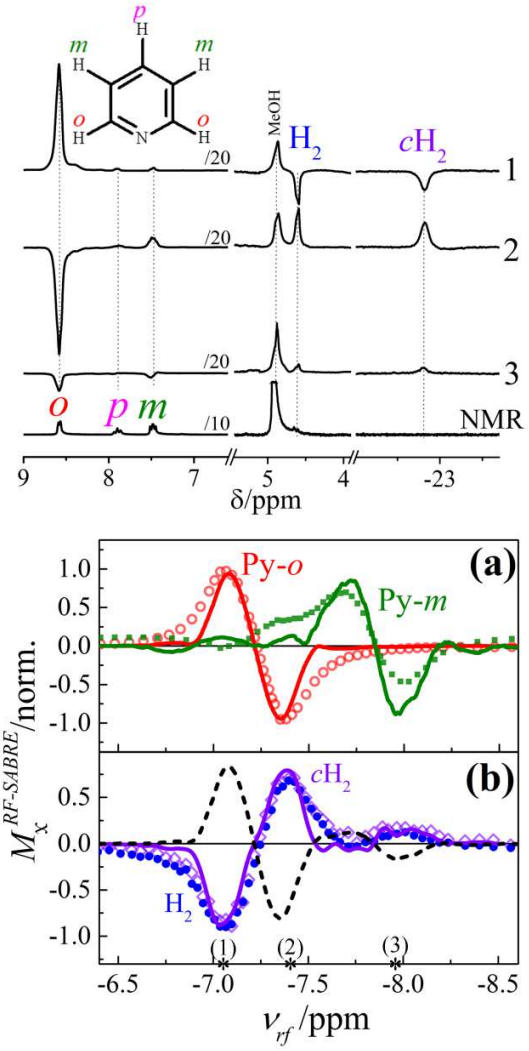

Figure 5. (top) ^{1}H RF-SABRE spectra of Py with the IrIMes in methanol obtained after applying an RF-field with amplitude of 28.6 kHz and frequency positions ν_{rf}=–7.0 ppm (curve 1), –7.4 ppm (curve 2), and –7.9 ppm (curve 3*).* Positions of different protons are assigned. Letters *o,p,m* denote the ortho, para and meta-protons of Py; H_2 and *c*H_2 denote dihydrogen in the bulk and at the active complex. The thermal single-scan NMR spectrum is also shown for comparison (bottom trace). (bottom) Dependence of the SABRE-derived NMR enhancement on ν_{rf} at amplitude ν_1=20.3 kHz for different protons is shown; asterisks denote ν_{rf} positions, for which RF-SABRE spectra (top) have been obtained. (a) Red: ortho-protons of py (Py-*o*), (b) magenta:

meta-protons of py (Py-*m*), green: para-proton of py (Py-*p*), (c) blue: dihydrogen in the bulk (H_2), violet: dihudrogen in active complex (cH_2). Lines show the simulation results for the 7-spin system of IrIMes with Py [H_2Ir–ePy] (see Table 4S (SI)). Maximal enhancement factors $\varepsilon = M_x^{RF-SABRE}/M_z^{thermal}(B_0 = 4.7\ T)$ are 52 for Py-*o*, 8 for Py-*m*, 150 for H_2 and 550 for cH_2.

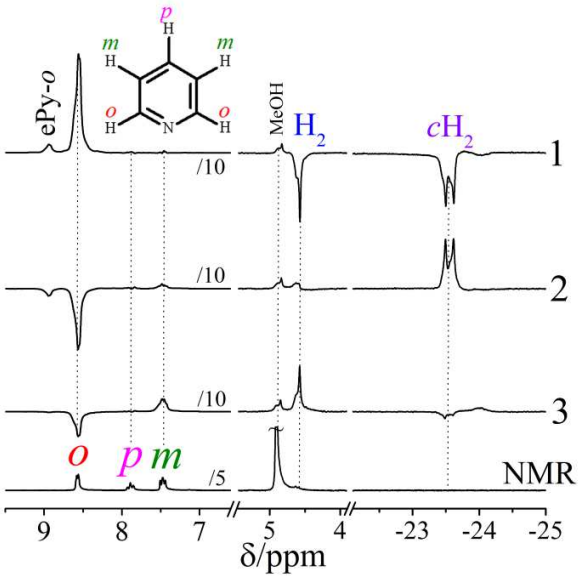

Figure 6. ^{1}H RF-SABRE spectra of Py with Crabtree's catalyst in methanol obtained after applying an RF-field with amplitude of 28.6 kHz and frequency positions at –7.15 ppm (trace 1), –7.50 ppm (trace 2) and –7.90 ppm (trace 3). The thermal single-scan NMR spectrum is also shown for comparison (bottom trace). Positions of different protons are assigned. Letters *o,p,m* denote the ortho, para and meta-protons of py; H_2 and *c*-H_2 denote dihydrogen in the bulk and in the catalyst.

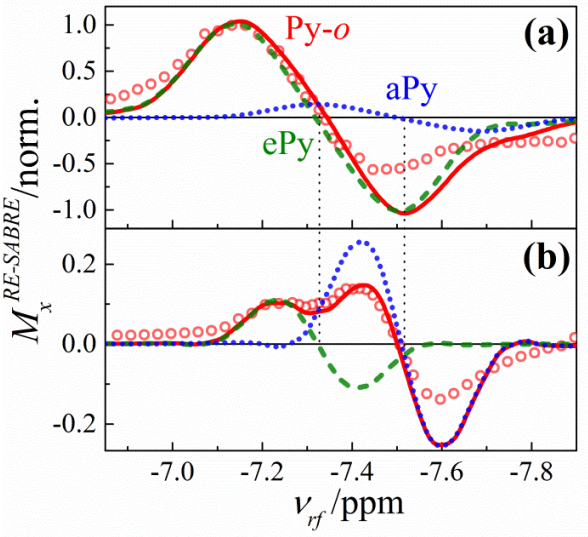

Figure 7. Dependence of NMR enhancement induced by RF-SABRE on ν_{rf} for different ν_1 values for the ortho-protons of Py in the system of Py with Crabtree's catalyst in methanol: 28.6 kHz (a) and 11.4 kHz (b). Lines show the simulation results: dashed green lines – calculation for the 8-spin system Crabtree [H_2PIr–ePy], dotted blue lines – calculation for the system Crabtree [H_2PIr–aPy], solid red line – sum of the two curves given by the dashed and dotted lines. Max enhancement factor $\varepsilon = M_x^{RF-SABRE}/M_z^{thermal}(B_0 = 4.7\ T)$ for Py-*o* is 45.

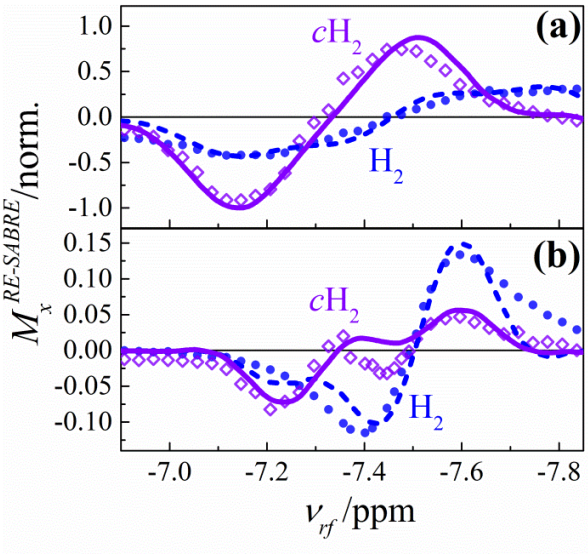

Figure 8. Dependence of NMR enhancement induced by RF-SABRE on ν_{rf} for different ν_1 values for the dihydrogen in the bulk (blue triangles: H_2) and dihydrogen in the active complex (violet diamonds: cH_2) in the system of Py with Crabtree's catalyst in methanol: 28.6 kHz (a) and 11.4 kHz (b). Lines show the simulation results for cH_2 and H_2 (see text). Maximal enhancement factors $\varepsilon = M_x^{RF-SABRE}/M_z^{thermal}(B_0 = 4.7\ T)$ are 180 for cH_2 and 80 for H_2.

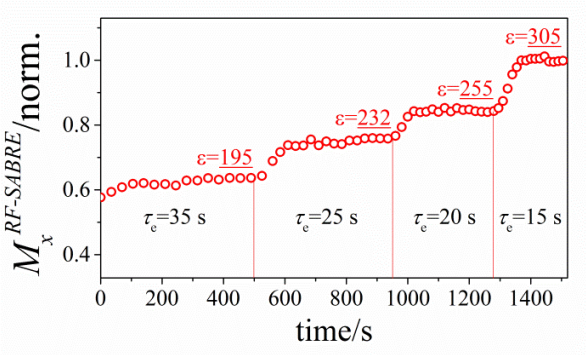

Figure 9. Continuous ^{1}H re-hyperpolarization at high field of 200 MHz NMR by means of RF-SABRE for 2,2′-bipyrazine with IrIMes in methanol. H3 proton is hyperpolarized. Here ν_1=28.6 kHz, ν_{rf}=–6.46 ppm, τ_{rf}=0.4 s, τ_b=10 s, by changing the time interval between the two consecutive bubbling stages the total duration of single RF-SABRE cycle, τ_e, was varied: 35s, 25 s, 20 s and 15 s.

REFERENCES

1. Zeng, H. F.; Xu, J. D.; McMahon, M. T.; Lohman, J. A. B.; van Zijl, P. C. M., Achieving 1% NMR Polarization in Water in Less than 1 Min Using SABRE. *J. Magn. Reson.* **2014,** *246*, 119-121.
2. Truong, M. L.; Shi, F.; He, P.; Yuan, B. X.; Plunkett, K. N.; Coffey, A. M.; Shchepin, R. V.; Barskiy, D. A.; Kovtunov, K. V.; Koptyug, I. V.; Waddell, K. W.; Goodson, B. M.; Chekmenev, E. Y., Irreversible Catalyst Activation Enables Hyperpolarization and Water Solubility for NMR Signal Amplification by Reversible Exchange. *J. Phys. Chem. B* **2014,** *118*, 13882-13889.
3. Theis, T.; Truong, M.; Coffey, A. M.; Chekmenev, E. Y.; Warren, W. S., LIGHT-SABRE Enables Efficient In-magnet Catalytic Hyperpolarization. *J. Magn. Reson.* **2014,** *248*, 23-26.
4. Pravdivtsev, A. N.; Yurkovskaya, A. V.; Vieth, H. M.; Ivanov, K. L., Spin Mixing at Level Anti-Crossings in the Rotating Frame Makes High-field SABRE Feasible. *Phys. Chem. Chem. Phys.* **2014,** *16*, 24672-24675.
5. Ivanov, K. L.; Pravdivtsev, A. N.; Yurkovskaya, A. V.; Vieth, H.-M.; Kaptein, R., The Role of Level Anti-Crossings in Nuclear Spin Hyperpolarization. *Prog. Nucl. Magn. Reson. Spectrosc.* **2014,** *81*, 1-36.
6. Barskiy, D. A.; Kovtunov, K. V.; Koptyug, I. V.; He, P.; Groome, K. A.; Best, Q. A.; Shi, F.; Goodson, B. M.; Shchepin, R. V.; Truong, M. L.; Coffey, A. M.; Waddell, K. W.; Chekmenev, E. Y., In Situ and Ex Situ Low-Field NMR Spectroscopy and MRI Endowed by SABRE Hyperpolarization. *ChemPhysChem* **2014,** *15*, 4100-4107.
7. Green, R. A.; Adams, R. W.; Duckett, S. B.; Mewis, R. E.; Williamson, D. C.; Green, G. G. R., The Theory and Practice of Hyperpolarization in Magnetic Resonance Using Parahydrogen. *Prog. Nucl. Magn. Reson. Spectrosc.* **2012,** *67*, 1-48.
8. Dücker, E. B.; Kuhn, L. T.; Münnemann, K.; Griesinger, C., Similarity of SABRE Field Dependence in Chemically Different Substrates. *J. Magn. Reson.* **2012,** *214*, 159-165.
9. Cowley, M. J.; Adams, R. W.; Atkinson, K. D.; Cockett, M. C. R.; Duckett, S. B.; Green, G. G. R.; Lohman, J. A. B.; Kerssebaum, R.; Kilgour, D.; Mewis, R. E., Iridium N-Heterocyclic Carbene Complexes as Efficient Catalysts for Magnetization Transfer from para-Hydrogen. *J. Am. Chem. Soc.* **2011,** *133*, 6134-6137.
10. Adams, R. W.; Aguilar, J. A.; Atkinson, K. D.; Cowley, M. J.; Elliott, P. I. P.; Duckett, S. B.; Green, G. G. R.; Khazal, I. G.; López-Serrano, J.; Williamson, D. C., Reversible Interactions with para-Hydrogen Enhance NMR Sensitivity by Polarization Transfer. *Science* **2009,** *323*, 1708-1711.
11. Pravdivtsev, A. N.; Yurkovskaya, A. V.; Vieth, H.-M.; Ivanov, K. L.; Kaptein, R., Level Anti-Crossings are a Key Factor for Understanding para-Hydrogen-Induced Hyperpolarization in SABRE Experiments. *ChemPhysChem* **2013,** *14*, 3327-3331.
12. Hövener, J. B.; Bär, S.; Leupold, J.; Jenne, K.; Leibfritz, D.; Hennig, J.; Duckett, S. B.; von Elverfeldt, D., A Continuous-flow, High-throughput, High-pressure Parahydrogen Converter for Hyperpolarization in a Clinical Setting. *NMR Biomed.* **2013,** *26*, 124-131.
13. Eshuis, N.; Hermkens, N.; van Weerdenburg, B. J. A.; Feiters, M. C.; Rutjes, F. P. J. T.; Wijmenga, S. S.; Tessari, M., Toward Nanomolar Detection by NMR Through SABRE Hyperpolarization. *J. Am. Chem. Soc.* **2014,** *136*, 2695-2698.

14. Eshuis, N.; van Weerdenburg, B. J. A.; Feiters, M. C.; Rutjes, F. P. J. T.; Wijmenga, S. S.; Tessari, M., Quantitative Trace Analysis of Complex Mixtures Using SABRE Hyperpolarization. *Angew. Chem., Int. Ed.* **2015,** *54*, 1481-1484.
15. Hövener, J. B.; Knecht, S.; Schwaderlapp, N.; Hennig, J.; von Elverfeldt, D., Continuous Re-hyperpolarization of Nuclear Spins Using Parahydrogen: Theory and Experiment. *ChemPhysChem* **2014,** *15*, 2451-2457.
16. Hövener, J. B.; Schwaderlapp, N.; Lickert, T.; Duckett, S. B.; Mewis, R. E.; Highton, L. A. R.; Kenny, S. M.; Green, G. G. R.; Leibfritz, D.; Korvink, J. G.; Hennig, J.; von Elverfeldt, D., A Hyperpolarized Equilibrium for Magnetic Resonance. *Nat. Commun.* **2013,** *4*, 2946.
17. Natterer, J.; Bargon, J., Parahydrogen Induced Polarization. *Prog. Nucl. Magn. Reson. Spectrosc.* **1997,** *31*, 293-315.
18. Zeng, H.; Xu, J.; Gillen, J.; McMahon, M. T.; Artemov, D.; Tyburn, J.-M.; Lohman, J. A. B.; Mewis, R. E.; Atkinson, K. D.; Green, G. G. R.; Duckett, S. B.; van Zijl, P. C. M., Optimization of SABRE for Polarization of the Tuberculosis Drugs Pyrazinamide and Isoniazid. *J. Magn. Reson.* **2013,** *237*, 73-78.
19. Barskiy, D. A.; Kovtunov, K. V.; Koptyug, I. V.; He, P.; Groome, K. A.; Best, Q. A.; Shi, F.; Goodson, B. M.; Shchepin, R. V.; Coffey, A. M.; Waddell, K. W.; Chekmenev, E. Y., The Feasibility of Formation and Kinetics of NMR Signal Amplification by Reversible Exchange (SABRE) at High Magnetic Field (9.4 T). *J. Am. Chem. Soc.* **2014,** *136*, 3322-3325.
20. Franzoni, M. B.; Graafen, D.; Buljubasich, L.; Schreiber, L. M.; Spiess, H. W.; Münnemann, K., Hyperpolarized H-1 Long Lived States Originating From Parahydrogen Accessed by rf Irradiation. *Phys. Chem. Chem. Phys.* **2013,** *15*, 17233-17239.
21. Pravdivtsev, A. N.; Yurkovskaya, A. V.; Lukzen, N. N.; Vieth, H. M.; Ivanov, K. L., Exploiting Level Anti-Crossings (LACs) in the Rotating Frame for Transferring Spin Hyperpolarization. *Phys. Chem. Chem. Phys.* **2014,** *16*, 18707-18719.
22. Atkinson, K. D.; Cowley, M. J.; Elliott, P. I. P.; Duckett, S. B.; Green, G. G. R.; López-Serrano, J.; Whitwood, A. C., Spontaneous Transfer of Parahydrogen Derived Spin Order to Pyridine at Low Magnetic Field. *J. Am. Chem. Soc.* **2009,** *131*, 13362-13368.
23. Kownacki, I.; Kubicki, M.; Szubert, K.; Marciniec, B., Synthesis, Structure and Catalytic Activity of the First Iridium(I) Siloxide versus Chloride Complexes with 1,3-mesitylimidazolin-2-ylidene ligand. *J. Organomet. Chem.* **2008,** *693*, 321-328.
24. Braunschweiler, L.; Ernst, R. R., Coherence Transfer by Isotropic Mixing: Application to Proton Correlation Spectroscopy. *J. Magn. Reson.* **1983,** *53*, 521-528.
25. Kiryutin, A. S.; Yurkovskaya, A. V.; Kaptein, R.; Vieth, H.-M.; Ivanov, K. L., Evidence for Coherent Transfer of para-Hydrogen-Induced Polarization at Low Magnetic Fields. *J. Phys. Chem. Lett.* **2013**, *4*, 2514-2519.
26. Korchak, S. E.; Ivanov, K. L.; Yurkovskaya, A. V.; Vieth, H.-M., Para-hydrogen Induced Polarization in Multi-spin Systems Studied at Variable Magnetic Field. *Phys. Chem. Chem. Phys.* **2009,** *11*, 11146-11156.
27. Ardenkjaer-Larsen, J. H.; Fridlund, B.; Gram, A.; Hansson, G.; Hansson, L.; Lerche, M. H.; Servin, R.; Thaning, M.; Golman, K., Increase in Signal-to-noise Ratio of > 10,000 Times in Liquid-state NMR. *Proc. Natl. Acad. Sci. U. S. A.* **2003,** *100*, 10158-10163.
28. Walker, T. G.; Happer, W., Spin-exchange Optical Pumping of Noble-gas Nuclei. *Rev. Mod. Phys.* **1997,** *69*, 629.
29. Batz, M; Nacher, P.-J.; Tastevin, G., Fundamentals of Metastability Exchange Optical Pumping. *J. Phys.: Conf. Ser.* **2011,** *294*, 012002.

30. Salikhov, K. M.; Molin, Y. N.; Sagdeev, R. Z.; Buchachenko, A. L., *Spin polarization and magnetic effects in chemical reactions*. Elsevier: Amsterdam, 1984.
31. Gafurov, M.; Denysenkov, V.; Prandolini, M. J.; Prisner, T. F., Temperature Dependence of the Proton Overhauser DNP Enhancements on Aqueous Solutions of Fremy's Salt Measured in a Magnetic Field of 9.2 T. *Appl. Magn. Reson.* **2012,** *43*, 119-128.
32. Denysenkov, V.; Prandolini, M. J.; Gafurov, M.; Sezer, D.; Endeward, B.; Prisner, T. F., Liquid State DNP Using a 260 GHz High Power Gyrotron. *Phys. Chem. Chem. Phys.* **2010,** *12*, 5786-5790.
33. Villanueva-Garibay, J. A.; Annino, G.; van Bentum, P. J. M.; Kentgens, A. P. M., Pushing the Limit of Liquid-state Dynamic Nuclear Polarization at High Field. *Phys. Chem. Chem. Phys.* **2010,** *12*, 5846-5849.

Table of Contents Graphic